Control, Operation, and Stability Characteristics of Grid-Forming Type III Wind Turbines

Preprint

Shahil Shah and Vahan Gevorgian

National Renewable Energy Laboratory

Presented at the 19th Wind Integration Workshop
November 11–12, 2020

NREL is a national laboratory of the U.S. Department of Energy
Office of Energy Efficiency & Renewable Energy
Operated by the Alliance for Sustainable Energy, LLC

This report is available at no cost from the National Renewable Energy Laboratory (NREL) at www.nrel.gov/publications.

Contract No. DE-AC36-08GO28308

Conference Paper
NREL/CP-5D00-78158
November 2020

Control, Operation, and Stability Characteristics of Grid-Forming Type III Wind Turbines

Preprint

Shahil Shah and Vahan Gevorgian

National Renewable Energy Laboratory

Suggested Citation
Shah, Shahil, and Vahan Gevorgian. 2020. *Control, Operation, and Stability Characteristics of Grid-Forming Type III Wind Turbines: Preprint*. Golden, CO: National Renewable Energy Laboratory. NREL/CP-5D00-78158.
https://www.nrel.gov/docs/fy21osti/78158.pdf.

Conference Paper
NREL/CP-5D00-78158
November 2020

National Renewable Energy Laboratory
15013 Denver West Parkway
Golden, CO 80401
303-275-3000 • www.nrel.gov

NOTICE

This work was authored by the National Renewable Energy Laboratory, operated by Alliance for Sustainable Energy, LLC, for the U.S. Department of Energy (DOE) under Contract No. DE-AC36-08GO28308. Funding provided by U.S. Department of Energy Office of Energy Efficiency and Renewable Energy Wind Energy Technologies Office. The views expressed herein do not necessarily represent the views of the DOE or the U.S. Government.

Cover Photos by Dennis Schroeder: (clockwise, left to right) NREL 51934, NREL 45897, NREL 42160, NREL 45891, NREL 48097, NREL 46526.

Control, Operation, and Stability Characteristics of Grid-Forming Type III Wind Turbines

Shahil Shah and Vahan Gevorgian
National Renewable Energy Laboratory (NREL), Golden, CO 80401, USA
Email: shahil.shah@nrel.gov, vahan.gevorgian@nrel.gov

***Abstract*—This paper explores the control, operation, and stability characteristics of grid-forming Type III wind turbines. The paper shows that the grid-forming operation mode requires the redesign of only the slower control loops for active and reactive power control, whereas the faster current control implementation can stay the same as grid-following wind turbines. The paper also shows that the operation of a wind turbine in the grid-forming mode results in higher mechanical stress because of the slower speed of the active power control. The paper compares the stability characteristics of the grid-forming and grid-following operation modes of Type III turbines by comparing the sequence impedance responses for both operation modes. It is found that the grid-forming operation mode substantially reduces the risks of subsynchronous oscillations between Type III wind turbines and series-compensated transmission lines. Moreover, the grid-forming Type III wind turbines can operate stably with extremely weak grids. The findings of this paper are demonstrated using PSCAD simulations of a 2.5-MW Type III wind turbine operating in grid-forming and grid-following modes.**

I. Introduction

Synchronous generators have served as the bedrock of electric power systems by providing voltage and angle stability at the fundamental frequency. They "form" the grid by acting as voltage sources and ensure that the frequency and magnitude of voltages at different nodes stay within a tolerable range of their nominal values. On the other hand, inverter-based resources (IBRs), such as wind and PV generators, operate in grid-following (GFL) mode by behaving as a current source feeding into the grid. Many studies, however, have identified that at least a portion of IBRs must operate in grid-forming (GFM) mode as their penetration increases to higher levels, reaching 100% [1].

Several installations of GFM inverter-based battery energy storage systems have been commissioned for microgrid and island applications [2], and a few are also integrated into bulk power system applications [3], [4]. GFM control of PV inverters and wind turbines is more difficult than that of storage inverters because of the lack of dispatchability in these resources. The implementation of GFM control in wind turbines is even more challenging than in PV inverters because of the complex dynamics of rotating generators and the aerodynamics of wind turbine rotors. Siemens Gamesa recently operated a small wind power plant with several 3.2-MW Type IV wind turbines operating in GFM mode using droop-based voltage and frequency control [5], [6]; however, there is very little information available on the operation of doubly-fed induction generator (DFIG) based Type III wind turbines in GFM mode. Type III wind turbines have a comparable share as Type IV wind turbines in terms of installed capacity, and they are preferred for land-based wind power plants; hence, it is important to evaluate the GFM operation mode for Type III wind turbines.

The electrical controls of Type III wind turbines operating in GFM mode are expected to be significantly more complex than those of Type IV wind turbines because the generator is directly connected to the grid, which basically requires the operation of the induction generator as a voltage source, similar to a synchronous generator. In addition to control, it is important to evaluate the operational characteristics of GFM wind turbines, which include addressing the following:

1) Whether the operation of a Type III wind turbine in GFM mode will increase the mechanical stress on the turbine
2) Whether the GFM operation will affect the average power production from the wind turbine
3) Whether additional storage and/or changes to the mechanical pitch control are required for the GFM mode; and
4) Whether the turbine can operate in maximum power point tracking (MPPT) mode or it must be operated with some curtailment.

Existing wind power plants using GFL wind turbines are prone to low-frequency stability problems when they operate under weak grid conditions [7], [8]. Moreover, wind power plants using GFL Type III wind turbines are also prone to SSO when they operate in close proximity of series-compensated transmission lines [9]. Hence, it is important to evaluate the stability characteristics of GFM Type III wind turbines to understand how they will perform with weaker grids and series-compensated transmission lines.

This paper explores these aspects of GFM Type III wind

This work was authored by Alliance for Sustainable Energy, LLC, the manager and operator of the National Renewable Energy Laboratory for the U.S. Department of Energy (DOE) under Contract No. DE-AC36-08GO28308. Funding provided by U.S. Department of Energy Office of Energy Efficiency and Renewable Energy Wind Energy Technologies Office. The views expressed in the article do not necessarily represent the views of the DOE or the U.S. Government. The U.S. Government retains and the publisher, by accepting the article for publication, acknowledges that the U.S. Government retains a nonexclusive, paid-up, irrevocable, worldwide license to publish or reproduce the published form of this work, or allow others to do so, for U.S. Government purposes.

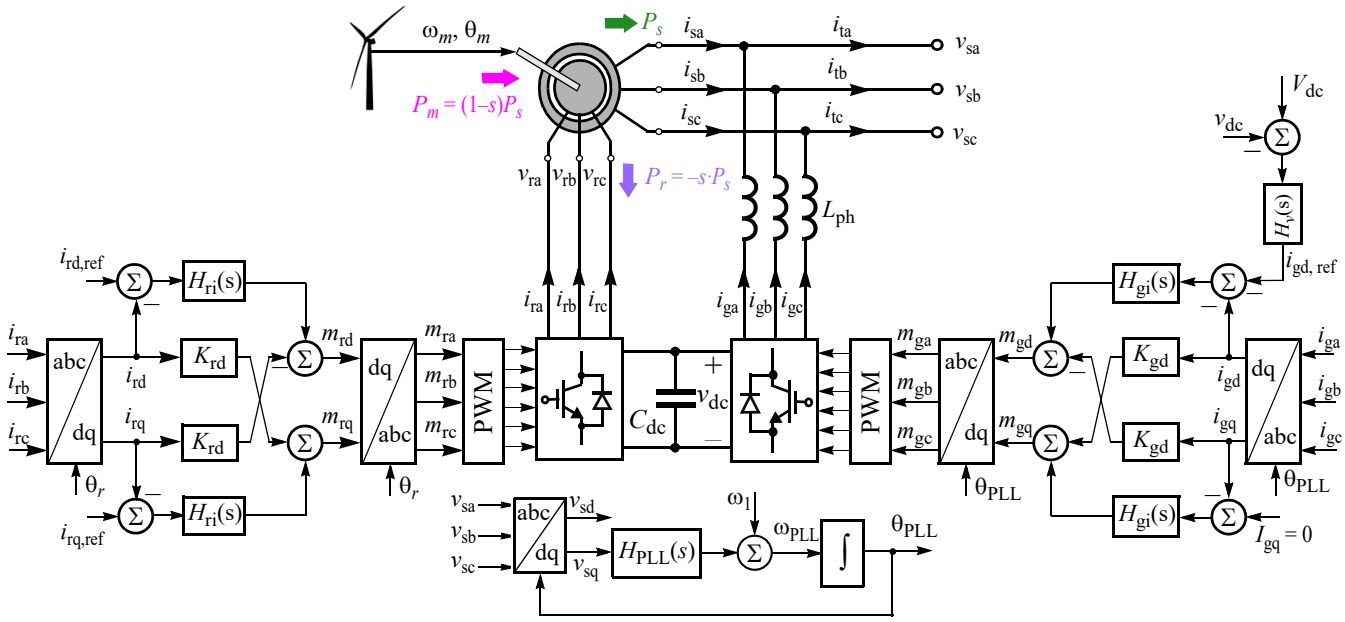

Fig. 1. DFIG-based Type III wind turbine with vector current control of RSC and GSC.

turbines. The paper first describes the control methods for realizing GFM capability in Type III turbines. It is shown that only the slower control loops need to be redesigned for the GFM control of Type III turbines. On the operational characteristics, the paper shows that the speed of the active power control of GFM turbines is slower than that of GFL turbines; this results in increased mechanical stress and could affect the annual power production from the turbine. These effects, however, can be mitigated to some extent using advanced pitch control. Finally, the stability characteristics of the GFM mode are compared with those of the GFL mode by comparing the sequence impedance responses of a Type III wind turbine for both operation modes. It is found that GFM Type III wind turbines have substantially lower risk of experiencing SSO problems than GFL Type III wind turbines. Moreover, the GFM mode allows stable operation of wind turbines with extremely weak grids; there might be stability issues, however, for operation with very strong grids.

The rest of the paper is organized as follows: Section II presents control methods for operating Type III wind turbines in the GFM mode. Section III and IV, respectively, discuss the operational and stability characteristics of GFM Type III wind turbines. Section V presents conclusions of this paper.

II. Turbine Control for GFL and GFM Modes

In the GFM mode, the turbine should behave as a voltage source and stay synchronized with the grid during small disturbances. The control methods for operating a DFIG-based Type III wind turbine as a voltage source can be classified broadly into two categories: vector control methods [10]–[12] and scalar control methods [13], [14]. Vector control methods are preferred for controlling DFIGs because of their superior performance and ability to ride-through fault events.

A. *Vector Current Control of DFIG*

Fig. 1 shows a DFIG with vector current control implemented in the back-to-back converters. The same implementation is used for the GFM and GFL operation modes. The d- and q-axis references for the grid-side converter (GSC) output currents, i_{gd} and i_{gq}, are derived, respectively, from the dc bus voltage and reactive power control loops. The q-axis reference, i_{gq}, in Fig. 1 is fixed at zero by assuming that no reactive power is supplied by the GSC. The grid voltage angle for the dq current control of the GSC is obtained using a phase-locked loop (PLL) for the GFL operation mode. The GFM operation mode can also use a PLL for the dq current control of the GSC because the main function of the GSC is to regulate the dc bus voltage, and its control does not influence the GFL or GFM behavior of the turbine. On the contrary, the outer control loops of the rotor-side converter (RSC) and the way the rotating reference frame for the vector control of the RSC is defined are key for operating the turbine in either the GFL or GFM operation modes.

B. *RSC Control for GFL Mode*

The outer control loops of the RSC for the GFL operation mode are shown in Fig. 2. The d- and q-axis references for the rotor currents, i_{rd} and i_{rq}, are obtained, respectively, from the active and reactive power control loops; this basically shows that the turbine will behave as a current source for controlling its power output. The angle of the rotating dq reference frame, with respect to the rotor winding axis, used for the vector control of the RSC is obtained using the PLL output, θ_{PLL}, and the rotor position with respect to the stator winding axis, θ_m:

$$\theta_r = \theta_{PLL} - \theta_m \tag{1}$$

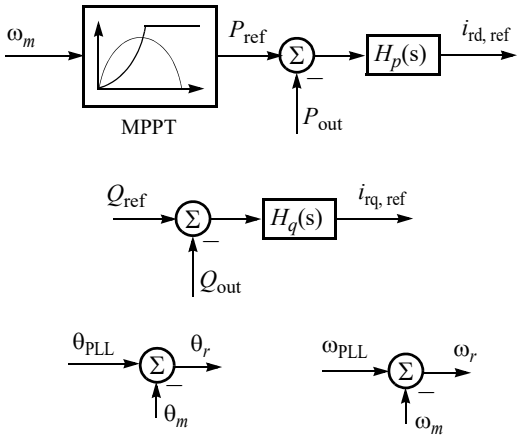

Fig. 2. Outer control loops of the RSC for GFL operation mode.

Basically the GFL operation mode relies on a PLL for synchronizing the induction generator output currents with the grid voltages.

C. RSC Control for GFM Mode

Fig. 3 shows the outer control loops of the RSC for operating a Type III wind turbine in GFM mode. It is evident that the control implementation is much more complicated for the GFM operation mode. As shown in Fig. 3a) and b), the active and reactive power control loops generate, respectively, the reference for the frequency, ω_s, and magnitude, v_m, of voltages at the stator terminals; hence, in GFM mode, the turbine will behave as a voltage source for controlling its power output.

For controlling the frequency of stator voltages, as shown in Fig. 3c), the stator frequency reference, $\omega_{s,\text{ref}}$, is used to generate angle, θ_r, of the rotating reference frame used for the vector current control of the RSC shown in Fig. 1. Note that the angle θ_r of the control reference frame is with respect to the rotor windings axis, which is also rotating at mechanical speed ω_m rad/s. The purpose of using θ_r that is derived from $\omega_{s,\text{ref}}$ is to control the frequency of the rotor currents such that the frequency of the stator voltages will track the reference $\omega_{s,\text{ref}}$. Note that, unlike the GFL mode, which uses a PLL for obtaining θ_r, the GFM mode uses an internal frequency reference for deriving θ_r.

For controlling the magnitude of stator voltages, as shown in Fig. 3b), the voltage control compensator $H_{\text{vm}}(s)$ generates reference for the magnetizing current of the induction generator, i_{sm}, depending on the error between the reference and measurement of the stator voltage magnitude: $v_{m,\text{ref}}$ and v_m, respectively. Basically the stator voltage magnitude is controlled by regulating the magnetic flux linking the stator windings. The magnetizing current of the induction generator, i_{sm}, is not directly measurable, but its reference can be used for developing reference for the q-axis component of the rotor currents, i_{rq}, as follows:

The d- and q-axis components of the stator flux in the rotating reference frame used for the vector control of the RSC can be

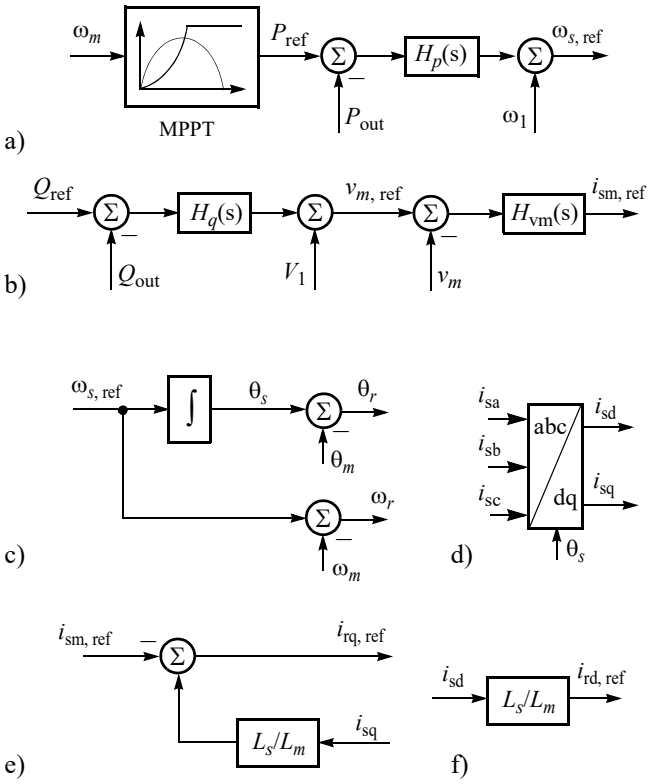

Fig. 3. Outer control loops of the RSC for GFM operation mode: a) active power control through stator frequency control, b) reactive power control through stator voltage magnitude control, c) position of dq reference frame for vector control of the RSC with respect to the stator windings axis, θ_s, and rotor windings axis, θ_r, d) d- and q-axis components of stator currents, e) reference for the q-axis component of the rotor currents, and f) reference for the d-axis component of the rotor currents.

written in terms of the stator and rotor current components as:

$$\begin{aligned} \psi_{\text{sd}} &= -L_s i_{\text{sd}} + L_m i_{\text{rd}} \\ \psi_{\text{sq}} &= -L_s i_{\text{sq}} + L_m i_{\text{rq}} \end{aligned} \tag{2}$$

Moreover, the stator voltage equation in the rotating reference frame can be written as [15]:

$$\begin{aligned} v_{\text{sd}} &= -R_s i_{\text{sd}} + \frac{d\psi_{\text{sd}}}{dt} - \omega_s \psi_{\text{sq}} \\ v_{\text{sq}} &= -R_s i_{\text{sq}} + \frac{d\psi_{\text{sq}}}{dt} + \omega_s \psi_{\text{sd}} \end{aligned} \tag{3}$$

The negative sign in front of the terms containing i_{sd} and i_{sq} in (2) and (3) is because of the source convention used for the stator currents in Fig. 1. For voltage-oriented control of the DFIG [15], the q-axis component of stator voltage, v_{sq}, is zero in steady-state. Based on (3), this implies that the d-axis component of the stator flux, Ψ_{sd}, should be zero in steady-state if the voltage drop across the stator winding resistance, R_s, is negligible. Similarly, the q-axis component of the stator flux in steady state can be obtained by using (3) and ignoring the voltage drop across the stator

winding resistance. The steady-state values of the d- and q-axis components of the stator flux for voltage-oriented control are given by [15]:

$$\Psi_{sd} = 0 \text{ and } \Psi_{sq} = -\frac{V_1}{\omega_s} \quad (4)$$

where V_1 is the steady-state value of v_{sd}, and it is the same as the amplitude of the phase voltages at the stator terminals.

The stator flux can be related with the magnetizing current, i_{sm}, and the dq-axis components of the stator currents using (2) as follows:

$$\psi_{sq} = -L_m i_{sm} = -L_s i_{sq} + L_m i_{rq} \quad (5)$$

Again, the negative signs in (5) are because the source convention is used for the stator currents. Eq. (5) is used to derive reference for i_{rq} in Fig. 3e) based on the reference for the magnetizing current, i_{sm}, as follows:

$$i_{rq,ref} = -i_{sm,ref} + \frac{L_s}{L_m} i_{sq} \quad (6)$$

It is important for the above described control method for regulating the frequency and magnitude of voltages at the generator terminals that the rotating reference frame used for vector control is locked with the stator voltages. As shown in (4), the d-axis component of the stator flux, Ψ_{sd}, must be zero for the reference frame aligned with the stator voltages. Hence, based on (2), the rotating reference frame can be locked with the stator voltages by regulating the d-axis component of the rotor currents to follow the reference:

$$i_{rd,ref} = \frac{L_s}{L_m} \cdot i_{sd} \quad (7)$$

To derive the d- and q-axis references for the rotor currents using (6) and (7), we need to obtain the dq-axis components of the stator currents, i_{sd} and i_{sq}. They are obtained using Park's transformation as shown in Fig. 3d). The angle of the rotating reference frame with respect to the stator windings axis, θ_s, required for implementing the Park's transformation, is obtained from the frequency reference, $\omega_{s,ref}$, as shown in Fig. 3c).

The active and reactive power controllers, $H_p(s)$ and $H_q(s)$, respectively in Fig. 3a) and b), can be implemented using proportional (P), integral (I), or proportional + integral (PI) control. The proportional control is equivalent to the droop control used in synchronous generators. With the proportional control, the error between the active and reactive power references and the actual power output of the turbine will be zero in steady state if the frequency and magnitude of grid voltages are fixed at the nominal values. On the other hand, the GFM turbine will provide primary frequency and voltage response by modulating its active and reactive power output whenever the frequency and magnitude of grid voltages move away from their nominal values. Note that a headroom is required for the wind turbine to provide primary frequency response by operating it at an off-MPPT power level; one method to maintain active power reserve is to use a de-loading curve instead of the MPPT curve for generating the active power reference depending on the rotor speed [11]. Unlike the proportional control, there will not be any steady-state errors between the active and reactive power references and the actual power output of the turbine, irrespective of the frequency and magnitude of grid voltages; hence, the GFM turbine will exactly follow its active and reactive power commands in steady state. However, it must be ensured that the active power reference is not higher than the maximum available power to avoid stability problems; such operation even during a transient condition can destabilize the wind turbine.

D. Pitch Control and Aerodynamics

The pitch control and aerodynamics of the wind turbine are kept the same for the GFL and GFM modes for comparison. The aerodynamics of the wind turbine are modeled based on a GE report on wind turbine modeling for power system studies [16]. The pitch control ensures that the wind turbine speed does not exceed 1.2 p.u.; it gets activated whenever the turbine speed starts increasing beyond 1.2 p.u., and it returns the rotor speed to 1.2 p.u. by increasing the pitch of the wind turbine blades. The pitch angle range is from 0^o to 25^o. The pitch angle stays at 0^o if the wind turbine rotor speed is less than 1.2 p.u., enabling the wind turbine to extract maximum power from the wind. Implementation of the aerodynamic model, MPPT control, and pitch control of the wind turbine in PSCAD is borrowed from [17].

III. Turbine Operation in GFL and GFM Modes

This section compares the operational characteristics of GFL and GFM modes using PSCAD simulations of a 2.5-MW Type III wind turbine. The RSC and GSC controls are implemented for both the GFL and GFM modes as described in the previous section. Fig. 4 shows the response of the wind turbine for the GFL and GFM modes when the wind speed is suddenly increased from 5 to 12 m/s at t = 10 s. As shown, for both the operation modes, the turbine responds to the change in the wind speed, and its power output increases from 0.4 MW to the rated level of 2.5 MW. However, the turbine reacts faster in the GFL mode, and its active power output quickly increases to 2.5-MW level. Moreover, as soon as the power output of the GFL turbine reaches 2.5 MW, it settles to the final value with minimum overshoot. Because the turbine operates as a current source in the GFL mode, its current output is quickly controlled to minimize overshoot beyond the rated power level. On the other hand, the power output of the turbine in the GFM mode increases at a slower rate than that of the GFL mode, and the turbine also experiences some overshoot. This is because the active power output of the turbine in the GFM mode is controlled by modulating the frequency of the stator voltages, which is an indirect control, and its response speed is also affected by the inertia of the induction generator.

As shown in Fig. 4, because the output power of the turbine in the GFM mode increases at a slower rate during a sudden jump in

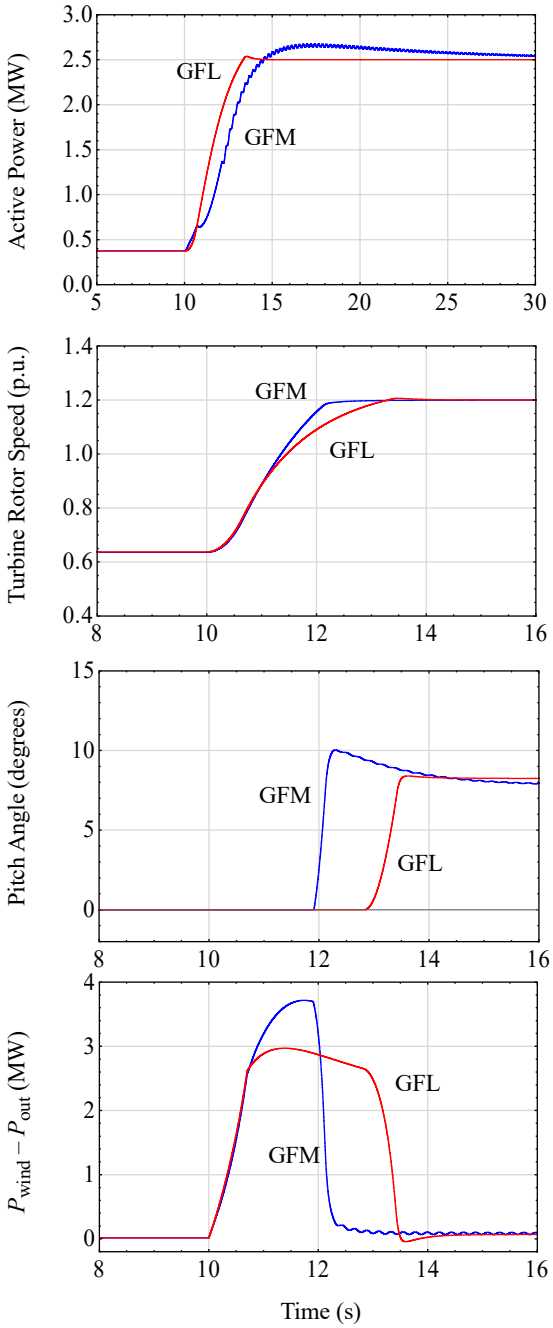

Fig. 4. Response of a 2.5-MW Type III wind turbine to a sudden change in wind speed from 5 to 12 m/s at t = 10 s for GFL and GFM operation modes.

the wind speed, the speed of the rotor will increase at a faster rate in the GFM mode because of the higher mismatch in the available aerodynamic power in the wind and the electrical power output of the turbine. Because of this, the pitch control of the turbine gets activated sooner in the GFM mode than in the GFL mode. The pair of traces in the bottom-most plot in Fig. 4 show that the mismatch between the aerodynamic power and the turbine power output increases to a higher value in the GFM mode than the GFL mode before it settles back to zero after the pitch control brings down the aerodynamic power.

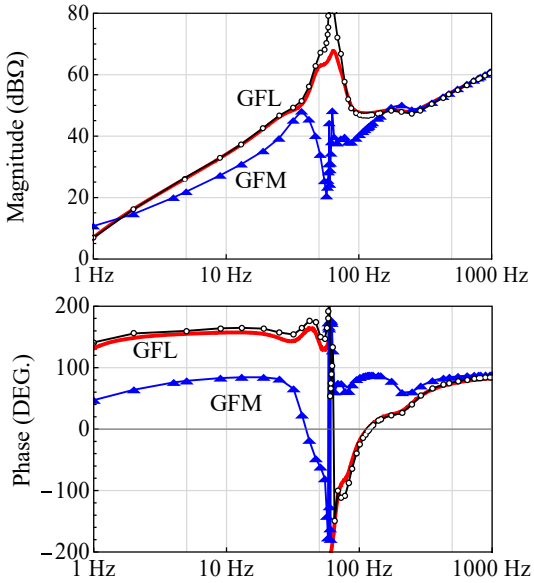

Fig. 5. Comparison of the positive-sequence impedance response, $Z_p(s)$, of a 2.5-MW Type III wind turbine for operation in GFM and GFL control modes. GFM mode: blue lines with triangles (simulations); GFL mode: black lines with circles (simulations) and red solid lines (analytical model).

This discussion shows that a wind turbine will face higher mechanical stress or a mismatch in the aerodynamic power and the turbine power output during transient conditions when it is operated in the GFM mode. This could impact the life of the wind turbine when it is operated in the GFM mode, but the quantification of this impact requires further investigation. It can also be inferred from the pitch angle response in Fig. 4 that the speed of the pitch control does not affect the additional mechanical stress faced by the wind turbine in the GFM mode; the pitch control reacts only after the wind turbine speed has reached the upper limit—1.2 p.u. in this case. The pitch control can be designed to respond to the power mismatch in addition to the turbine speed to reduce the power mismatch and hence the mechanical stress on the turbine during transient conditions. There might be challenges, however, in estimating the power mismatch in real-time and such advanced pitch control might also reduce the power production from the wind turbine.

IV. Stability of Grid-Forming Type III Turbines

A. *Subsynchronous Oscillations*

Impedance-based methods have proven effective for evaluating the stability of IBRs under different grid conditions and their impact on the stability of bulk power systems, mainly because they do not depend on white-box models of IBRs [18]. Fig. 5 compares the positive-sequence impedance response of the 2.5-MW Type III wind turbine when it is operated in GFM and GFL modes. Note that the phase response of the impedance in Fig. 5 for the GFL mode is higher than +90° at subsynchronous

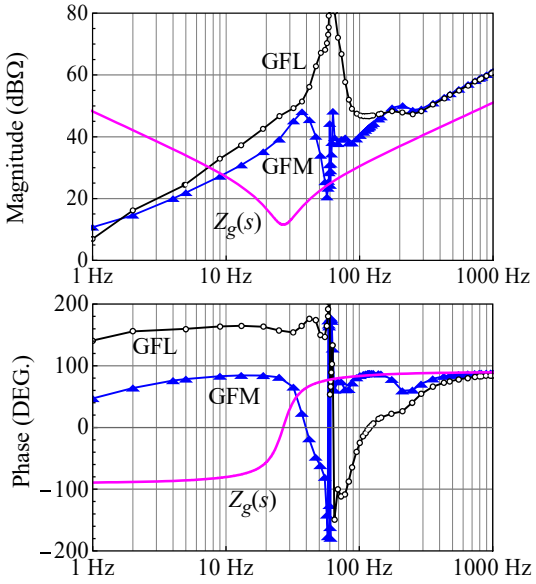

Fig. 6. Comparison of the positive-sequence impedance response of a 2.5-MW Type III wind turbine operating in GFM and GFL control modes with the impedance of the grid at its terminals, $Z_g(s)$. The grid consists of a series-compensated line with 20% compensations.

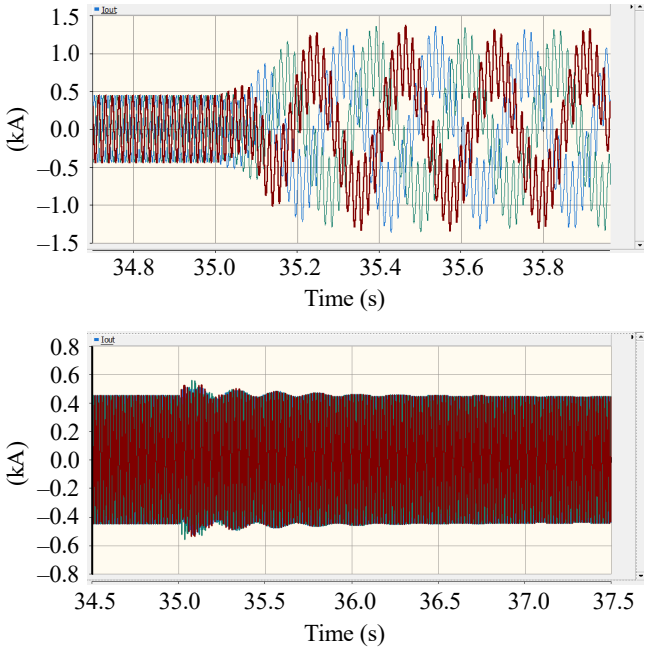

Fig. 7. Output currents of a 2.5-MW Type III turbine when it is supplying to a series-compensated transmission line. The compensation capacitors are inserted at t = 35 s. Upper traces: GFL operation mode; lower traces: GFM operation mode.

frequencies; this signifies negative resistance or damping at subsynchronous frequencies, which could result in SSO when the a wind power plant with such turbines supplies directly to a series-compensated transmission line. On the other hand, Fig. 5 shows that for the same physical design, pitch control, and aerodynamics, the turbine does not exhibit negative resistance or

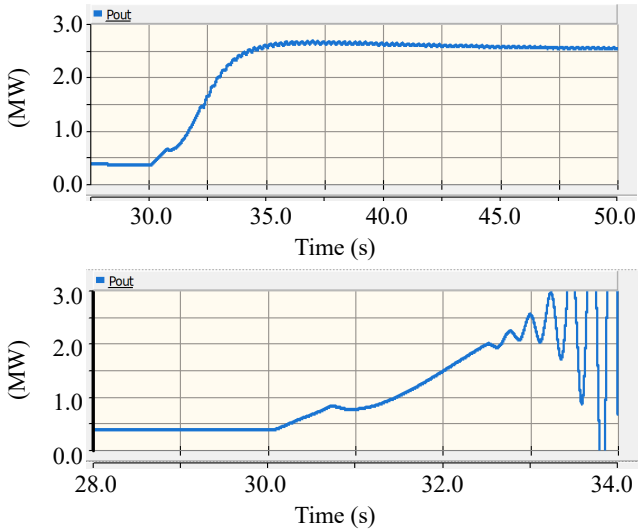

Fig. 8. Output power of a 2.5-MW Type III wind turbine operating in the GFM mode during a sudden change in wind speed from 5 to 12 m/s at t = 30 s. Grid SCR is 4 (weak grid) for the upper trace and it is 8 (strong grid) for the lower trace.

damping at subsynchronous frequencies when it is operated in the GFM mode. This shows that Type III wind turbines are less likely to experience SSO problems when they are operated in the GFM mode. Fig. 6 compares the positive-sequence impedance response of the 2.5-MW wind turbine when it is operated in GFM and GFL modes with the impedance response of the grid with a series-compensated transmission line with 20% compensation. Following the principles of the impedance-based stability analysis [18], [19], it can be inferred from Fig. 6 that the turbine forms an unstable subsynchronous resonance (SSR) mode at 8 Hz with the series-compensated transmission line when it is operated in the GFL mode. On the other hand, the turbine forms a stable SSR mode at 10 Hz when it is operated in the GFM mode. Indeed, PSCAD simulations of the turbine shown in Fig. 7 confirm that its operation in the GFL mode with a series-compensated line will result in SSO, whereas it will operate stably with the series-compensated line when it is operated in the GFM mode. Fig. 5 also shows the impedance response of the 2.5-MW turbine for the GFL operation mode obtained using a mathematical model presented in [9]. We will develop a similar model for the sequence impedance of Type III wind turbines for operation in the GFM mode; it will explain the fundamental factors that make GFM Type III wind turbines less likely to experience the SSO problems with series-compensated transmission lines.

B. Impact of Grid Strength

Fig. 8 shows the active power output of the 2.5-MW wind turbine during a sudden change in wind speed from 5 to 12 m/s when it is operated in the GFM mode for two different grid conditions. The simulations are performed for two different values of grid strength: first when the grid short-circuit ratio (SCR) is 4 and second when it is 8. It is evident that the GFM

turbine becomes unstable for the stronger grid. On the other hand, the GFM turbine operates stably when the grid is weaker with the SCR of 4. In fact, we have seen in PSCAD simulation studies that the GFM turbine can operate stably with an extremely weak grid and that it can also operate in stand-alone mode and supply local loads. This is because of the voltage source behavior of the GFM turbine. Because of its voltage source characteristics, GFM wind turbines require a certain amount of impedance between the wind plant and the grid. The stability problem with GFM wind turbines appears only for very strong grids, and it can be easily avoided by inserting reactors in front of the turbines or using high-impedance turbine transformers to maintain a certain grid impedance under all operating conditions.

V. Conclusion

In this paper, we presented the control, operation, and stability characteristics of GFM Type III wind turbines and compared them with the standard GFL Type III wind turbines. The paper showed that the GFM mode can use the same pitch control and vector control current as the GFL turbine; the GFM mode is implemented through slower outer control loops that regulate the active and reactive power output of the turbine by modulating, respectively, the frequency and magnitude of voltages at the generator terminals. The paper showed that the speed of the active power control is slower in the GFM operation mode, which could result in increased mechanical stress on the turbine than a similar GFL turbine. The impact of more mechanical stress on the life of the turbine, mitigation solutions, and their potential impact on average power production requires further investigation. By comparing the positive-sequence impedance response of a Type III wind turbine for operation in the GFL and GFM modes, the paper showed that a GFM Type III wind turbine is less likely to suffer from SSO problems when it is operated with series-compensated transmission lines. The paper also showed that GFM wind turbines can operate stably with extremely weak grids, but they may experience low-frequency stability problems under very strong grid conditions. This behavior is opposite to the GFL wind turbines, which are prone to low-frequency oscillations during operation with weaker grids.

Acknowledgments

The authors thank Jian Fu of the US Department of Energy's Wind Energy Technologies Office for her feedback and continuous support of this project.

References

[1] B. Kroposki, B. Johnson, Y. Zhang, V. Gevorgian, P. Denholm, B. Hodge, and B. Hannegan, "Achieving 100% renewable grid," *IEEE Power and Energy Mag.*, March/April 2017.

[2] O. Schomann, "Experiences with large grid-forming inverters on various island and microgrid projects," in *Proc. Hybrid Power Systems Workshop*, May 2019, Crete, Greece. [Online]. Available: https://www.sma.de/en/products/references/st-eustatius-caribbean.html

[3] Large-Scale Battery Storage Knowledge Sharing Report, *prepared by Aurecon for Australian Renewable Energy Agency (ARENA)*, Sep. 2019. [Online]. Available: https://arena.gov.au/assets/2019/11/large-scale-battery-storage-knowledge-sharing-report.pdf

[4] *Inverter-Based Resource Workshop*, Electric Reliability Council of Texas (ERCOT), April 2019. [Online]. Available: http://www.ercot.com/content/wcm/key_documents_lists/176763/ERCOT_IBR_Workshop_April_25_2019.pdf

[5] A. Roscoe, et. al., "Practical experience of operating a grid-forming wind park and its response to system events," in *Proc. 18th Wind Intgr. Workshop*, Dublin, Ireland, Oct. 2019.

[6] A. Roscoe, et. al., "Practical experience of providing enhanced grid forming services from an onshore wind park," in *Proc. 19th Wind Integr. Workshop*, Nov. 2020 (to be published).

[7] S.-H. Huang, J. Schmall, J. Conto, J, Adams, Y. Zhang, ad C. Carter, "Voltage control challenges on weak grids with high penetration of wind generation: ERCOT experience," in *Proc. 2012 IEEE Power Energy Soc. Gen. Meeting (PESGM)*, San Diego, CA.

[8] L. Fan and Z. Miao, "An explanation of oscillations due to wind power plants weak grid interconnection," *IEEE Trans. Sustain. Energy*, vol. 9, no. 1, pp. 488-490, Jan. 2018.

[9] S. Shah, V. Gevorgian, and H. Liu, "Impedance-based prediction of SSR-generated harmonics in doubly-fed induction generators," in *Proc. 2019 IEEE Power Energy Soc. Gen. Meeting (PESGM)*, Atlanta, GA.

[10] R. Pena, J. C. Clare, and G. M. Asher, "A doubly fed induction generator using back-to-back PWM converters supplying an isolated load from a variable speed wind turbine," *Proc. Inst. Electr. Eng.—Electrical Power Applications*, vol. 143, no. 4, pp. 380-387, Sep. 1996.

[11] L. Huang, H. Xin, L. Zhang, Z. Wang, K. Wu, and H. Wang, "Synchronization and frequency regulation of DFIG-based wind turbine generators with synchronized control," *IEEE Trans. Energy Conv.*, vol. 32, no. 3, pp. 1251-1262, Sep. 2017.

[12] A. K. Jain and V. T. Ranganathan, "Wound induction generator with sensorless control and integrated active filter for feeding nonlinear loads in a stand-alone grid," *IEEE Trans. Ind. Electron.*, vol. 55, no. 1, pp. 218-228, Jan. 2008.

[13] S. Wang, J. Hu, and X. Yuan, "Virtual synchronous control for grid-connected DFIG-based wind turbines," *IEEE. J. Emerg. Sel. Topics Power Electron.*, vol. 3, no. 4, pp. 932-944, Dec. 2015.

[14] G. Iwanski and W. Koczara, "Sensorless direct voltage control of the stand-alone slip-ring induction generator," *IEEE Trans. Ind. Electron.*, vol. 54, no. 2, pp.1237-1239, April 2007.

[15] G. Abad, J. Lopez, M. A. Rodriguez, L. Marroyo, and G. Iwanski, *Doubly-Fed Induction Machine – Modeling and Control for Wind Energy Generation*. Piscataway, NJ: IEEE Press/John WILEY and Sons, 2011.

[16] K. Clark, N. W. Miller, and J. Sanchez-Gazca, "Modeling of GE wind turbine generators for grid studies," GE Energy, Ver. 4.5, General Electric International, Inc., One River Road, Schenectady, NY, April 16, 2010.

[17] "Type 3 Wind Turbine Model – written for PSCAD X4 version 4.6," PSCAD, Winnipeg, Canada, Revision 3, Nov. 2018 [Online]. Available: https://hvdc.ca/uploads/knowledge_base/type_3_wind_turbine_-model.pdf?t=1542818424. Accessed on: Dec. 27, 2019.

[18] S. Shah, et. al., "Impedance methods for analyzing stability impacts of inverter-based resources," in *Proc. 2nd National Science Foundation (NSF) Workshop on Power Electronics-Enabled Operation of Power systems*, Oct. 31–Nov. 1, 2019, Chicago, IL. [Online]. Available: https://www.nrel.gov/docs/fy20osti/75345.pdf

[19] S. Shah and L. Parsa, "Impedance modeling of three-phase voltage source converters in DQ, sequence, and phasor domains," *IEEE Trans. Energy Conv.*, vol. 32, no. 3, pp. 1139-1150, April 2017.